

# Mechanism of carbon nanotube growth by CVD

Roman Brukh, Somenath Mitra \*

*Department of Chemistry and Environmental Science, New Jersey Institute of Technology, Newark, NJ, USA*

Received 7 February 2006; in final form 23 March 2006

Available online 22 April 2006

## Abstract

The carbon nanotubes (CNTs) formation by catalytic chemical vapor deposition is initiated by precursor decomposition to form a multitude of reactive species. During large-scale CNT self-assembly, these species vary with residence time leading to a non-uniform CNT growth. This Letter studies the self-assembly, and the reaction pathways leading to CNT formation. A tubular plug flow reactor, where CNT deposition occurred at various residence times was used to study the process, and kinetic simulation was used to predict the reaction pathways. There was excellent agreement between experimental and the modeling results, providing an insight into the mechanism of CNT growth.

© 2006 Elsevier B.V. All rights reserved.

## 1. Introduction

Since their discovery in 1991 [1] carbon nanotubes (CNTs) have been the subject to intense research with potential applications [2–8] ranging from sensors [9,10] to hydrogen storage [11]. CNTs are usually synthesized by laser ablation of carbon rods [12], direct current arc-discharge between electrodes [13], or by chemical vapor deposition (CVD) [14,15]. While the first two techniques are appropriate for large-scale production of CNTs, they cannot be used for self-assembly on surfaces. CVD appears to be the method of choice for direct deposition on specific structures and substrates.

The synthesis of CNTs (single- or multiple-walled) by CVD involves the catalytic decomposition of a carbon precursor (e.g., CO, hydrocarbons, or alcohol) on nanostructured transition metal catalyst like Co, Ni, or Fe. Typical CVD temperatures vary between 600 and 1000 °C. The process is sensitive to the catalyst structuring, as well as to the reaction conditions. Nanotubes synthesized by CVD are known to be longer than those obtained by other

processes. It is also possible to grow dense arrays of aligned CNTs [16–18] by CVD.

The rate of deposition of CNTs and other non-tubular carbons (NTCs), such as, amorphous carbon and graphite depends on process/reaction conditions, the catalyst, and the precursor. During large-scale CNT self-assembly, where the CNTs are grown in a large structure, the gas-phase composition of the carbon source varies as active free radicals and intermediates at high temperature react with the precursor and among themselves. Modeling and simulations of such systems are needed for understanding their scale-up. In particular, kinetic models can be used to interpret precursor decomposition, intermediates, free radical formation, byproduct generation and in identifying the reaction pathways. Previous studies have mainly dealt with CNT self-assembly on small substrates, where many of these effects did not play significant roles. Extensive literature exists regarding the role of catalyst, carbon source and temperature effects [19–23], but very few describe the reaction mechanisms [24,25].

The objective of this Letter is to study the mechanism of CNT self-assembly and reaction pathways leading to CNT and NTC deposition. A tubular plug flow reactor, where CNT and NTC deposition occurred at various residence

\* Corresponding author.

E-mail address: [Mitra@njit.edu](mailto:Mitra@njit.edu) (S. Mitra).

times was used to study the process, and kinetic simulation was used to predict the reaction pathways.

## 2. Experimental

The experimental system [11] consisted of a programmable 12" long and 2.5" in diameter tube furnace (Lindberg model 847). The plug flow reactor comprises a 1.27 mm ID tubing into which CNT self-assembly took place. This was placed inside a quartz tube. Ethylene was used as the carbon source. The iron of the tubing steel served as the catalyst. The process has been described in details previously [10,11].

The entire CVD process consisted of two steps, namely, catalyst preparation and CNT deposition. The preparation step included the oxidation of the inside surface by flowing air for 30 min at 500 °C, followed by reduction by H<sub>2</sub> at the same temperature for an additional 30 min. This resulted in the formation of nano-structured catalyst on the tube surface [11]. The CVD step was carried out at 700 °C for 1, 5 and 15 min. During the deposition, the gaseous carbon source thermally decomposed/pyrolyzed inside the tubing. This resulted in the formation of active free radicals, a range of hydrocarbon species and elemental carbon. The latter deposited on the metal surface in form of CNT and NTC.

Several 1 cm long samples were cut at the different distances from the tube inlet. Each corresponded to a different residence time and different gas phase compositions of active species. The samples were analyzed by a scanning electron microscope (Leo 1530 VP, Carl Zeiss SMT AG Company, Germany).

## 3. Modeling methods

The gas-phase pyrolysis of the carbon source was modeled and simulated using the CHEMKIN [26]. Here, the tubing served as a plug flow reactor. At steady-state, the governing species balance equations in the tubing were calculated by a set of differential equations:

$$\frac{dY_k}{dt} = \frac{\omega_k W_k}{\rho} \quad (1)$$

where  $Y_k$  was the mass fraction of specie  $k$ ,  $t$  was the residence time,  $\omega_k$  was the net molar rate of production (ROP) by reaction of specie  $k$ ,  $W_k$  was molecular weight of species  $k$  and  $\rho$  was the density of the pyrolyzed carbon source. The residence time,  $t$ , was related to the volume of the tubing,  $V$  and the total feed mass flow rate,  $G$ , by equation:

$$t = \frac{\rho V}{G} \quad (2)$$

where the density  $\rho$  was calculated from the ideal gas law:

$$\rho = \frac{P\bar{W}}{RT} \quad (3)$$

where  $P$  was the pressure (one atmosphere),  $\bar{W}$  was the mean molecular weight of the pyrolyzed gas mixture,  $R$

the universal gas constant and  $T$  was the absolute temperature.

The net production rate of a specie  $k$ ,  $\omega_k$ , was determined as a function of concentration and temperature with the aid of the provided reaction mechanism [27] and temperature. The former comprises a set of reversible elementary gas phase reactions with rate constants and corresponding thermodynamic properties.

To determine the contribution of each reaction to the production or destruction of species, the ROP analysis was performed. The net generation and the destruction rates of species, including breakdowns of these net rates into the rates of each contributing reaction were computed. The net molar ROP by reaction  $\omega_k$  of a specie  $k$  was calculated as:

$$\omega_k = \sum_{i=1}^I v_{ki} q_i \quad (4)$$

where  $q_i$  was the rate of progress for the reaction  $i$ . The normalized ROP,  $C_{ki}$ , to the ROP of species  $k$  from reaction  $i$  was calculated from:

$$C_{ki} = \frac{v_{ki} q_i}{\sum_{i=1}^I v_{ki} q_i} \quad (5)$$

The value of  $C_{ki}$  showed how reaction  $i$  contributed to the formation, or consumption of species  $k$ . This information was used for the identification of production and destruction pathways for the species.

## 4. Results and discussion

The purpose of this Letter was to investigate the self-assembly of carbon nanotubes in a plug flow mode, and relate their formation to the kinetics of precursor pyrolysis. The films of CNT and NTC were simultaneously deposited inside the stainless steel tubing, which has been presented in our previous publications [10,11,28]. Based on Raman spectroscopy data, no single wall tubes were observed and only multiple walled CNTs were present. Typical nanotube growth is shown in Fig. 1. The C<sub>2</sub>H<sub>4</sub> decomposed to form elemental carbon, which then assembled as CNTs or NTC on the tube surface. The CNTs were aligned radially. The NTC appeared to deposit on top of the CNTs (Fig. 1a), and could be selectively removed by oxidation in the presence of oxygen at 250–300 °C [28]. Residual CNT layer after NTC removal is shown in Fig. 1b.

The mechanism of nanotube formation is hypothesized to be as follows. First the C<sub>2</sub>H<sub>4</sub> decomposed to produce free radicals, which in presence of the iron catalyst formed CNTs. Once the catalyst was exhausted, the NTC formation occurred. Active free radicals are also known to recombine with carbon to form larger molecules [29]. So, on one hand the carbon formed in the gas phase was deposited on the metal surface, at the same time the carbon was consumed to form secondary products. As the residence

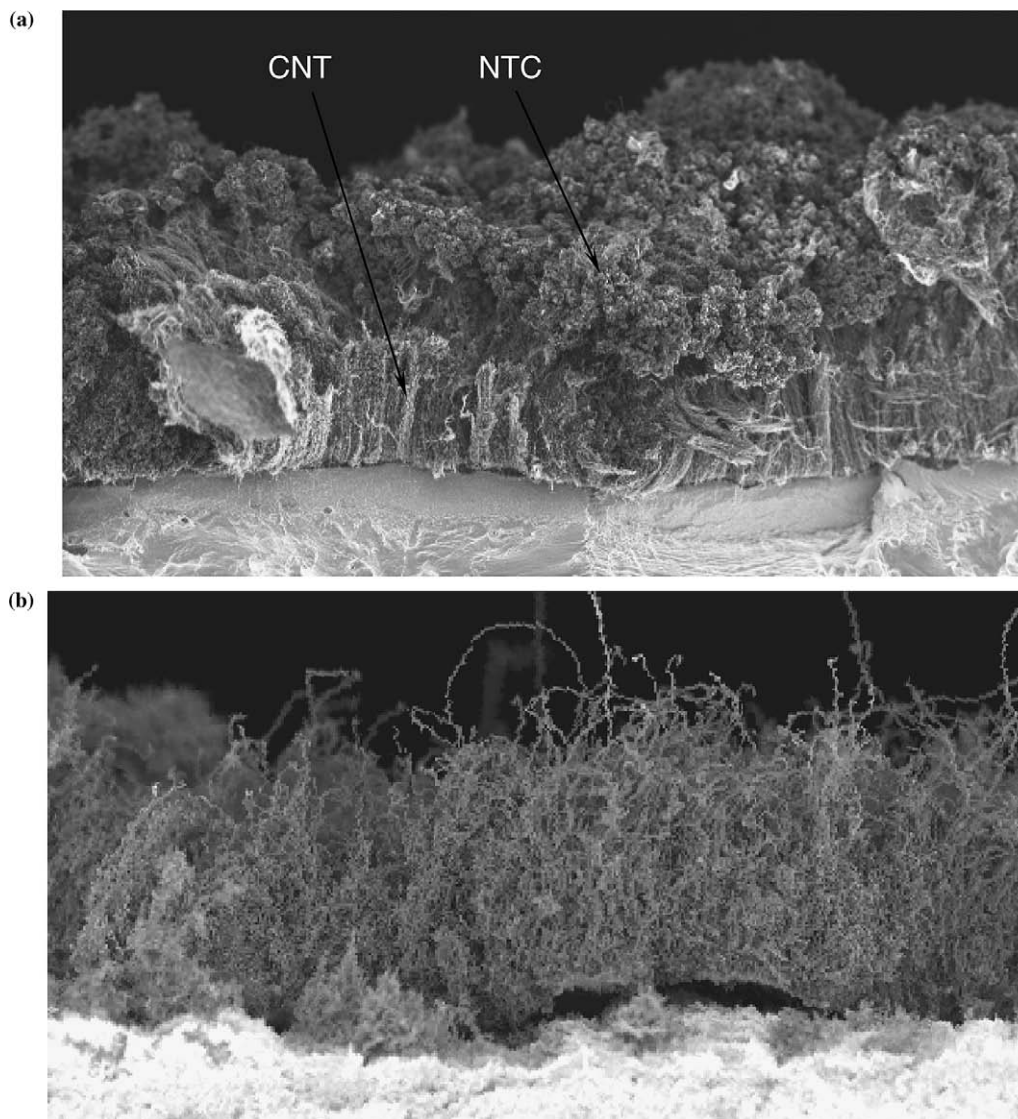


Fig. 1. (a) CNTs covered by NTC; (b) CNTs after the removal of NTC by oxidation (2000 $\times$ , 1 mm = 0.5  $\mu$ m).

time along the tube increased, the concentrations of the active species changed, leading to a variability of the thicknesses of both the CNTs and NTC films [11].

#### 4.1. Model predictions

Based on CHEMKIN simulation, at residence time about 0.005 s, which corresponded to a location near the tube entrance, the major reaction was the decomposition of  $C_2H_4$  to form acetylene ( $C_2H_2$ ) via:



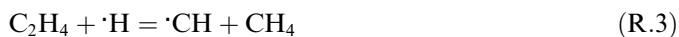
This then reacted with hydrogen radical ( $\cdot H$ ) to form vinyl radical ( $\cdot CH_3$ ) and elemental carbon (C), which could end up as either CNT or NTC:



At this residence time, the rate of C consumption was negligible, and it deposited to form nanotubes and NTC. The

pathways to  $C_2H_4$  consumption and C production are shown in Fig. 2a. The rates of production and consumption of gas phase elemental carbon are shown in Fig. 3a.

As the pyrolyzed gas traveled along the tube, further decomposition of hydrogen containing species resulted in an increase in  $\cdot H$  concentration. At this point, the attack of  $\cdot H$  on  $C_2H_4$  became the major reaction leading to  $C_2H_4$  destruction. Thus, C formation at a residence time of 0.1 s was dependent on  $\cdot H$ :



This is shown in Fig. 2b. At residence times between 0.1 and 0.2 s, reaction (R.3) produced nearly 100% of the  $\cdot CH$ , which reacted with  $\cdot H$  to provide 100% of the C via reaction (R.4).

As the residence time increased, the concentrations of active radicals and intermediates in the gas phase increased, they began to recombine, and formed larger

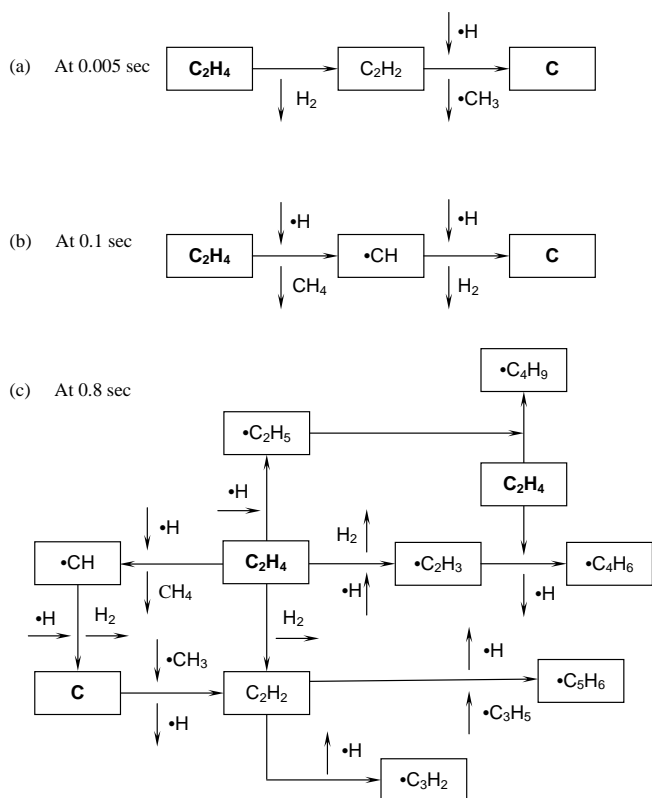


Fig. 2. Major pathways to consumption of  $C_2H_4$  and production/consumption of C at different residence time.

molecules. Under these conditions, active radicals consumed the available C that would have otherwise formed CNTs and NTC. As shown in Fig. 3a, at residence times between 0.3 and 0.6 s, the rate of gas phase consumption of C increased sharply, and the net rate of carbon production decreased. At residence time higher than 0.6 s, the original carbon supplying specie  $\cdot CH$  combined with other intermediates, such as,  $C_2H_2$  and  $H_2$  to form larger molecules:



At these conditions, reactions (R.5) and (R.6) consumed 43% and 54% of all available  $\cdot CH$ , respectively. Radicals and intermediates reacted among each other, with  $C_2H_4$ , and led to molecular growth according to:



Reactions (R.7)–(R.10) consumed about 33%, 10%, 35%, and 6% of the remaining  $C_2H_4$  respectively, while only 10% of available  $C_2H_4$  molecules at  $t = 0.9$ – $1.0$  s decomposed according to reaction (R.1) to form  $C_2H_2$ , most of which was involved in the molecular growth by

reactions (R.5) and (R.11). Moreover, almost all  $\cdot C_2H_3$  formed by R.7 (about 98%), further combined with  $C_2H_4$  according to R.9 to form larger molecules. Fig. 3b shows that the relative contribution of the reactions responsible for molecular growth ((R.7)–(R.10)) to the consumption of ethylene, which increased significantly with the increase in ethylene residence time. At the same time, the contribution of R.1 decreased rapidly. The major pathways to  $C_2H_4$  consumption and C formation at  $t = 0.8$  s are shown in Fig. 2c. GC–MS analysis of the gas exiting the tube at residence time around 0.9–1.2 s showed significant concentrations of high molecular weight species, such as, 1,3-butadiene, cyclopentene, 3-penten-1-yne, 1-pentene, 1,4-pentadiene, 2-hexane, hexane, 3-methyl-cyclopentene, benzene, 5-methyl-1,3-cyclopentadiene, 1,3-cyclohexadiene, cyclohexene. This confirmed molecular growth by the radical recombination.

#### 4.2. Effect of flow rate

The effect of flow rate on the thickness of the CNT and NTC films along with the computed carbon production and consumption rates is shown in Fig. 3a. The duration of CVD was 15 min. The thicknesses of CNT and NTC films varied along the length. Significant amount of NTC were observed at each flow rate. At all flow rates, the maximum film thickness was observed at residence time in the range of 0.3–0.7 s. The agreement between model prediction and experimental data is evident. The total amount of deposited carbon, which can be estimated by integrating the film thickness over the entire length increased with the increase in flow rate of the carbon source. At the low  $C_2H_4$  flow rate, such as 5 ml/min, the total amount of deposited carbon was less than that at flow rates 10 or 20 ml/min. This is due to the smaller amount of  $C_2H_4$  consumed during the 15 min CVD. Fig. 4 shows the carbon deposition per mole of  $C_2H_4$  used. The deposition efficiency appeared to be maximum at 10 ml/min.

The precursor flow rate determines its residence time and the gas phase species composition along the tube. Therefore, different carbon sources are expected to have different optimal flow rates.

#### 4.3. Effect of CVD time

CVD deposition of CNTs was carried out for 1, 3.5, 5 or 15 min at a  $C_2H_4$  flow rate of 20 ml/min. Then five samples were cut at 1, 10, 20, 30 and 40 cm from the front end of the tubing. These corresponded to residence time 0.0125, 0.125, 0.25, 0.375 and 0.5 s, respectively. The thicknesses of the CNT and NTC films were measured. The rates of growth of these films were calculated as the slopes of the thickness functions:

$$\text{Rate} = \frac{d\delta}{d\tau}$$

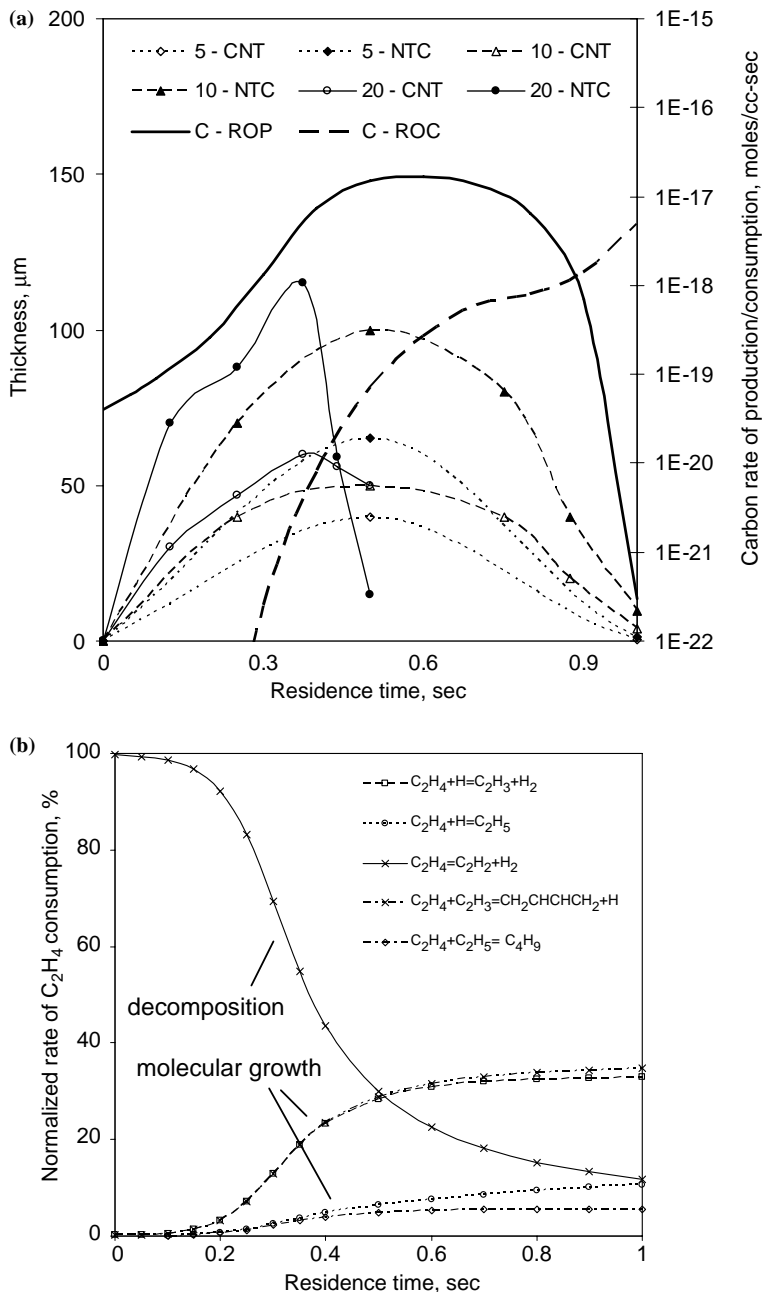


Fig. 3. (a) The thicknesses of CNT and NTC overcoat films as functions of  $\text{C}_2\text{H}_4$  residence time at flow rates of 5, 10 and 20 ml/min. CVD time 15 min [11]. Superimposed are rates of production and consumption of gas-phase carbon as a functions of the residence time; (b) Relative rate of consumption of  $\text{C}_2\text{H}_4$  as a function of gas phase residence time.

where  $\delta$  is the CNT or NTC film thickness and  $\tau$  is the CVD time. The films thickness and their growth rates as functions of the CVD duration are summarized in Figs. 5a and b, for residence times of 0.25 and 0.5 s, respectively. The others are not presented here for brevity. As shown, the structure and composition of the CNT and NTC films formed varied with residence time, as well as the CVD durations. For example, the film formed during the first minute of deposition contained significantly more CNT than NTC. With the increase in deposition time, the thickness of the CNTs increased, but the NTC film increased more rapidly.

Residence time played an important role. At low residence times during the first minute only CNTs were formed with practically no NTC. For example (Fig. 5a), at a residence time of 0.25 s, and a CVD time of 1 min, a 10  $\mu\text{m}$  thick CNT film was formed before NTC began to deposit on top. However, at residence time of 0.5 s, CNT and NTC growth started as soon as CVD was initiated. At a residence time of 0.25 s, as CVD time increased, relatively more NTC were formed, and the thickness of this layer was more than CNT layer. It was quite the opposite at a residence time of 0.5 s. It is clear that CNT and NTC formation mechanisms were different at these residence times.

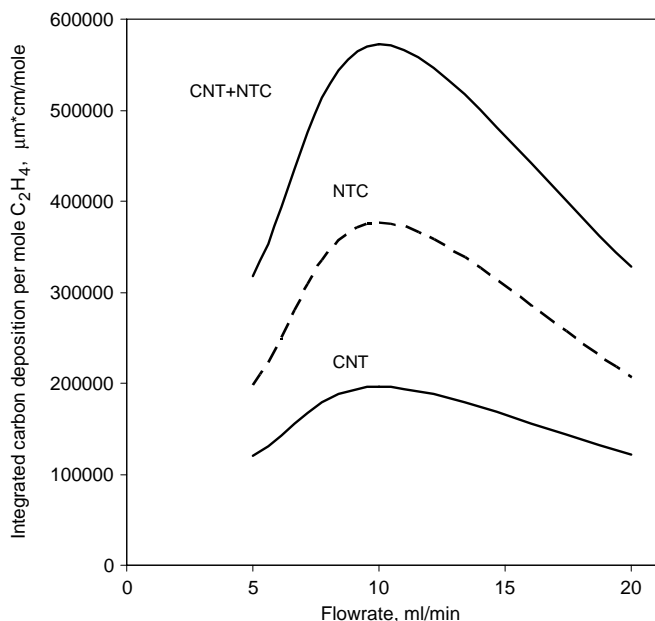


Fig. 4. Carbon deposited per mole of precursor as a function of flow rate.

Fig. 5b shows that the rate of growth of both CNT and NTC were different at different residence times. The rates increased with CVD time and then decreased.

These observations are important, because the goal is to selectively grow CNTs and prevent the growth of NTC. The CNT formation was associated with the availability of catalyst, and the NTC formation was due to the absence of it. This could be explained using the vapor–liquid–solid mechanism of CNT growth [30]. In the initial stages of CVD, the carbon atoms formed in the gas phase dissolved in the metal, and their concentration reached the solubility limit. The CNTs started to grow to cover the metal surface. With the increase in the CNT length and film thickness, the access to the catalytically active surface became limited, and the rate of CNT growth decreased. When the rate of gas phase carbon production exceeded the rate of carbon consumption by CNT formation, the carbon began to congregate as NTC on a top of the CNTs. The crucial role of catalyst availability for CNT nucleation has been reported by Unalan and Chhowalla [31] during the CNT deposition using ethanol. They observed the increased growth of amorphous carbon as soon as the availability of the catalyst decreased. This is in line with our observations.

As shown in Fig. 5b, at short residence times (less than 0.5 s) the growth rates of CNTs and NTCs were higher. At shorter residence time (0.25 s) the growth rate of CNT was initially higher than NTC, but then the latter grew at faster rate. However, at the longer residence time, the CNT deposition rate was higher irrespective of the residence time. This was again due to the availability of the catalyst. At low residence time (Fig. 5a), the CNT film was significantly thicker thus decreasing the access to the catalyst and lowering the rate of CNT formation. The kinetic model agreed with the experimental results presented in Figs. 3a and 5,

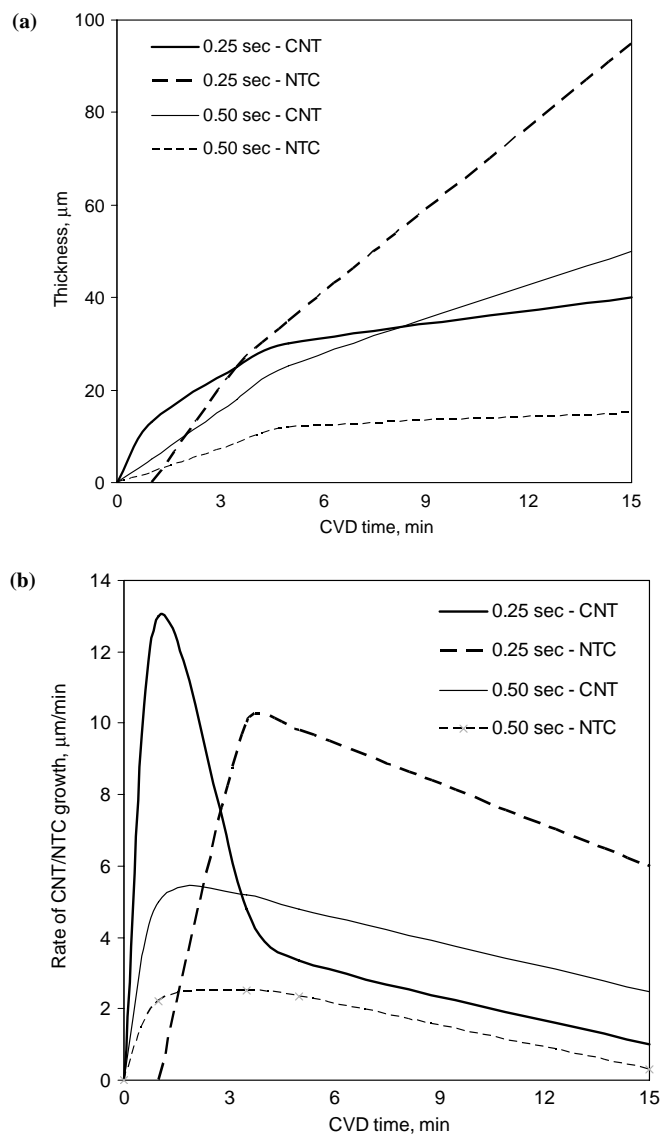


Fig. 5. The thicknesses and the growth rates of CNTs and NTC as a function of CVD time.  $C_2H_4$  flow rate is 20 ml/min.

which show that in the sections of the tubing corresponding to the residence time of 0.4 s, the film thickness reached their maximums.

It is prudent to suggest that the gas phase composition at short residence time, when  $C_2H_4$  decomposition along with the formation of low molecular weight species prevail, is more favorable for CNTs formation. At these conditions, the rate of C production is not too high and probably is the limiting factor in the CNT growth. Our experiments have shown that at high flow rate, 300 ml/min that corresponds to the total residence time of 0.01 s, amorphous carbon was not formed at all. The high rate of carbon production at  $t = 0.3$ – $0.4$  s exceeded its rate of consumption as CNTs, and led to the formation of amorphous carbon. In the portions of tubing that corresponded to even longer residence times ( $t = 1$ – $1.5$  s), where the formation of higher molecular weight hydrocarbons dominated, the rate of carbon consumption

by these reactions exceeded the rate of its formation, and the thickness of either CNT or NTC was found to be negligible.

## 5. Conclusion

The CVD precursor ( $C_2H_4$ ) decomposed to form elemental carbon via a sequence of free radical reactions, which then assembled as CNTs or NTC. The CNTs were aligned radially, and the NTC appeared to deposit on top of it. As the pyrolyzed gas traveled along the tube, the composition of active species changed, leading to variable thickness of the CNT and NTC films. At all flow rates; the maximum film thickness was observed in the residence time range of 0.3–0.7 s, and this agreed with the model predictions. The rate of carbon consumption leading to molecular growth increased with residence time. The rate of growth of both CNT and NTC were different at different residence times. The selective CNT formation was attributed to the availability of the catalyst, and NTC formation to the absence of it. It is clear that the selective growth of CNTs with respect to NTC would require the optimization of all these parameters.

## References

- [1] S. Iijima, *Nature* 354 (1991) 56.
- [2] H. Dai, J.H. Hafner, A.G. Rinzler, D.T. Ccbert, R.E. Smalley, *Nature* 384 (1996) 147.
- [3] Q.H. Wang et al., *Appl. Phys. Lett.* 72 (1998) 2912.
- [4] S. Fan et al., *Science* 283 (1999) 512.
- [5] C.J. Lee et al., *Appl. Phys. Lett.* 75 (1999) 1721.
- [6] M.M.J. Treacy, T.W. Ebbesen, J.M. Gibson, *Nature* 381 (1996) 678.
- [7] S.J. Tans, R.M. Verschueren, C. Dekker, *Nature* 393 (1999).
- [8] P. Pancharal, Z.L. Wang, D. Ugarte, W. de Heer, *Science* 283 (1999) 1513.
- [9] P.G. Collins, K. Bradley, M. Ishigami, A. Zeatl, *Science* 287 (2000) 1801.
- [10] C. Saridara, R. Brukh, Z. Iqbal, S. Mitra, *Anal. Chem.* 77 (2005) 1183.
- [11] M. Karwa, Z. Iqbal, S. Mitra, *Carbon* 44 (2006) 1235.
- [12] A.C. Dillon et al., *Nature* 386 (1997) 337.
- [13] A. Thess et al., *Science* 273 (1996) 483.
- [14] S. Iijima, T. Ichihashi, *Nature* 363 (1993) 609.
- [15] R. Andrews, D. Jacques, A.M. Rao, F. Derbyshire, D. Qian, X. Fan, E.C. Dickey, J. Chen, *Chem. Phys. Lett.* 303 (1999) 467.
- [16] M. Terrones et al., *Nature* 388 (1997) 52.
- [17] D.B. Geohegan, A.A. Puzos, I.N. Ivanov, S. Jesse, G. Eres, *Appl. Phys. Lett.* 83 (2003) 1851.
- [18] A.V. Melechko, V.I. Merkulov, T.E. McKnight, M.A. Guillorn, K.L. Klein, D.H. Lowndes, M.L. Simpson, *J. Appl. Phys.* 97 (2005).
- [19] L. Yuan, K. Saito, C. Pan, F.A. Williams, A.S. Gordon, *Chem. Phys. Lett.* 340 (2001) 237.
- [20] R.L. Vander Wal, L.J. Hall, *Combust. Flame* 130 (2002) 27.
- [21] M.A. Ermakova, D.Y. Ermakov, A.L. Chuvilin, G.G. Kuvshinov, *J. Catal.* 201 (2001) 183.
- [22] Z. Li, J. Chen, X. Zhang, Y. Li, K.K. Fung, *Carbon* 40 (2002) 409.
- [23] T. Hiraoka, T. Kawakubo, J. Kimura, R. Taniguchi, A. Okamoto, T. Okazaki, T. Sugai, Y. Ozeki, M. Yoshikawa, H. Shinohara, *Chem. Phys. Lett.* 382 (2003) 679.
- [24] H. Endo, K. Kuwana, K. Saito, D. Qian, R. Andrews, E.A. Grulke, *Chem. Phys. Lett.* 387 (2004) 307.
- [25] M. Grujicic, G. Cao, B. Gersten, *Appl. Surf. Sci.* 191 (2002) 223.
- [26] R.J. Kee, F.M. Rupley, J.A. Miller, SAND89-8009B, 1993.
- [27] N.M. Marinov, W.J. Pitz, C.K. Westbrook, M.J. Castaldi, S.M. Senkan, *Combust. Sci. Technol.* (1996).
- [28] C. Saridara, S. Mitra, *Anal. Chem.* 77 (2005) 7094.
- [29] R. Brukh, T. Salem, T. Slanvetpan, R. Barat, S. Mitra, *Adv. Environ. Res.* 6 (2002) 359.
- [30] O. Louchev, Y. Sato, H. Kanda, *Appl. Phys. Lett.* 80 (2002) 2752.
- [31] H.E. Unalan, M. Chhowalla, *Nanotechnology* 16 (2005) 2153.